Analysis of Planar and Spherical Shock-Wave Mitigation by Wet Aqueous Foams

C. Breda, S. Kerampran, M.-O. Sturtzer, M. Arrigoni and J.-F. Legendre

1 Introduction

In a context where more and more Improvised Explosive Devices (IED) are found on national territories or theaters of external operations, the fight against IEDs has intensified since 2008, aiming, in particular, at designing reliable blast mitigation systems. Aqueous foams were identified in the 1970s as an efficient protective medium against blast and sound effects. They have been widely used because of their ease of application, but the quantification of the physical phenomena leading to mitigation remains unclear. This study proposes to analyze the interaction with foam and either a spherical shock wave (pyrotechnic tests) or a planar shock wave (shock tube experiments), varying both the foam and the wave properties.

Winfield and Hill [1] performed experiments with 0.9 kg TNT charges located in a 3 m^3 volume of dry foam with a density 10 kg m^{-3}. They reached the conclusion that the blast peak overpressure and the positive impulse are reduced, respectively, by 95% and 75%. Similar experiments were performed by Hartman et al. [2] with C4 charges (TNT equivalent ranging from 0.25 to 25 kg) and Domergue et al. [3] with plastrite charges, yielding comparable results. McCallen [4], Hartman [2], and Del Prete [5] established empirical relations for overpressures, impulses, and times of arrival for foam densities ranging from 2 to 40 kg m^{-3} and for scaled distances from the charge from 0.7 to 2 kg $m^{-\frac{1}{3}}$.

Some attempts have been made to propose a theoretical model of blast wave attenuation by diphasic media, and in particular by aqueous foams. For instance, assuming the foam can be considered as an equivalent gas with modified thermodynamical

C. Breda · S. Kerampran (✉) · M. Arrigoni
IRDL, ENSTA Bretagne, Brest, France
e-mail: steven.kerampran@ensta-bretagne.fr

C. Breda · M.-O. Sturtzer · J.-F. Legendre
Institut Franco-allemand de Saint Louis, St. Louis, France

K. Kontis (ed.), *Shock Wave Interactions*,
https://doi.org/10.1007/978-3-319-73180-3_22

properties, and denoting ϵ the liquid fraction, Gelfand [6] expressed the ratio between overpressures P^* in the foam and P in air as a function of heat capacity and density

$$\frac{P^*}{P} = (1 + \gamma\mu\delta)^{-0.5}$$

with

$\delta = \frac{c_{p,l}}{c_{p,g}}$ the ratio of the heat capacity of the phases
$\mu = \frac{\epsilon\rho_l}{(1-\epsilon)\rho_g}$ the mass loading factor.

Studies have not been limited to evaluating the attenuation of the wave. The influence of some parameters has also been taken into consideration, in order to better design the foam confinement. Authors seem to agree on the fact that wet foams ($5\% < \epsilon < 30\%$) are more efficient than dry foams. The importance of the foam density has been experimentally evidenced: it is more efficient to increase the foam density than the foam thickness [7–9]. The available experimental data make it possible to roughly design a confinement. McCallen [4] established some empirical rules (using 100 kg charges in a foam volume of 2500 m^3 with a density of about 40 kg m^{-3}), stating for example that if the aqueous foam is heavier than the explosive charge by a factor ten, the resulting overpressure is divided by two.

Attention has also been paid to the structure of a shock or blast wave propagating in wet aqueous foams. Concerning blast waves, Borisov [10] differentiates two cases, depending on the ratio of the transmitted wave velocity in the foam (D) to the sound velocity of the gas contained in the foam bubbles (a):

- if $D < a$: the transmitted shock in the foam is divided in two successive compression waves:
  - a precursor wave, responsible for the foam liquid films rupture in droplets.
  - a main compression wave, which accounts for most of the overpressure and progressively accelerates the droplets until they reach an equilibrium state defined by a stationary pressure. This wave propagates at a lower velocity than the precursor.
- if $D > a$: the transmitted wave in the foam exhibits a single front, with no precursor.

Britan [8] and Del Prete [5] performed shock tube experiments to analyze the shock structure in a wet aqueous foam and concluded that it is similar to the one observed with blast waves. A double structure is observed, with a bell-shaped overpressure profile linked to a compression zone (from t_p to t_c), preceded by a precursor wave characterized by a sharp rise (from t_a to t_p), as depicted in Fig. 1. This precursor is the signature of the foam fragmentation in smaller droplets and the compression then accelerates droplets into an equilibrium between the gaseous and liquid phases. Britan [11] visualized the atomization phenomena in shock tubes and identified two cases depending on the density of the foam. When the impedance mismatch at the

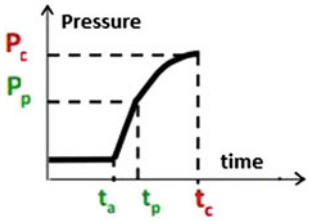

Fig. 1 Characteristic overpressure profile in an aqueous foam

air–foam boundary is close to unity, the precursor pressure (P_p) is close to transmitted pressure in the foam (P_c). But when the impedance mismatch is larger than one, the precursor pressure is noticeably lower than the transmitted pressure.

Because of its peculiar structure, aqueous foam is able to mitigate shock waves through the dissipation of kinetic energy. Indeed, such a medium is characterized by the following properties:

- a high compressibility of the gaseous phase in the bubbles
- a high heat capacity of the liquid phase, which can behave as a thermal sink
- a low sound velocity, relatively to the sound velocity in the gaseous and liquid phases
- a visco-elastic mechanical behavior [12].

During the shock–foam interaction, several physical phenomena can account for the overpressure mitigation:

- dissipation (heat, viscous, acoustic) [13–17]
- dispersion due to the wave reflection on the bubbles [13, 15–19]
- thickening of the shock front [15, 20, 21]
- partial transmission of shock at the foam–air interface [9, 14, 22]
- drainage, which increases the non-homogeneity of the foam in the direction perpendicular to the shock propagation and causes transverse effects leading to an increase of the shock obliquity [11, 22]
- pulsation and resonance of the bubbles [16, 17]
- fragmentation of foam into smaller droplets which absorb energy in the form of heat [5, 10, 12, 15].

The quantification of the relative effects of these phenomena is still unclear. Several authors differentiate two cases as a function of a nondimensional thickness X defined as [7, 8, 23, 24]:

$$X = d\left(\frac{\rho_m}{m_{ch}}\right)^{\frac{1}{3}}$$

with

ρ_m the foam density
m_{ch} the explosive mass TNT equivalent
$d = \frac{(lwh)^{\frac{1}{3}}}{2}$

l, w, h the dimensions of foam confinement.

Close to the charge ($X < 2.5$), the foam is completely destroyed. The liquid fraction and the foam density play dominant roles. The acceleration and heating of the resulting droplets are the consequence of the interaction between the foam and the blast. The single-phase model or the Effective Gas Flow model (EGF) can represent this case. The foam is considered as a gas with an effective adiabatic index that allows to take into account the real water content of the foam [10, 12, 17]. Far from the charge ($X > 2.5$), the foam can sustain the impact. Shattering of the shock wave at the bubbles, viscous dissipation at solid boundaries, bubble pulsation, and thermal conduction are the dominant mechanisms of the foam–blast interaction. It seems intuitively that as the foam becomes drier, the role of the pulsation increases and the viscous dissipation enhances the wave mitigation.

As can be seen, the topic of shock mitigation by aqueous foams has drawn some attention over the past decades. Nonetheless, this phenomenon is still only partially understood and despite some reliable experimental studies, the influence of some of the foam properties is still unclear. This can in part be attributed to insufficient characterization of the foam in the aforementioned studies and to the fact that large-scale studies make it difficult to accurately analyze the phenomenon. The present work has two main goals. We first aim at complementing the existing experimental results, both for blast and shock waves. We also study the so far mostly overlooked influence of the bubble size on the shock mitigation. In this respect, we performed experiments using both explosive charges and shock tubes, focusing on the control and accurate evaluation of the aqueous foam properties.

2 Foam Generation and Characterization

Wet aqueous foams (i.e., with densities larger than 50 kg m^{-3}) were chosen for this study, on the basis of the available experimental results. A bibliographical review indeed showed that previous works were mostly concerned with dry foams, which present a more regular structure than wet foams and can more easily be produced in a reproducible way. Yet, it appears that acoustic waves are better attenuated in wet foams. Besides, wet foams seem to be able to slow down the fragments generated by the detonation of an explosive device more efficiently (the interaction between supersonic projectiles and aqueous foams will be presented in a forthcoming paper).

Several requirements have to be fulfilled by the foam in order to ensure the quality of the results:

- foam production needs to be reproducible enough, i.e., the foam density must not vary by more than 20% from one test to the other,
- the foam must be monodisperse, which implies a polydispersity coefficient lesser than 0.5. This is particularly important since the bubble size is taken as a parameter.

- the foam must be stable in time, with a density that does not vary by more than 10% of its initial value after 30 min.

To generate foam, one needs a foaming liquid (obtained by mixing water and a foaming agent), a gas supply (air in the present case) and a generating device. The bubble size is highly dependent on the generating device. Since we intend to evidence the influence of the bubble diameter on the shock mitigation, we need to use different devices, in order to produce foams with significantly different mean bubble diameters. The foaming agent was selected among a panel of industrial agents designed for fire safety. These products are far from the academic foaming agents usually used, but have better properties with respect to stability. Eight preselected foaming agents were submitted to the Bikermann test, which consists in generating a foam with a sintered diffuser plunged into the foaming liquid and measuring the foam height in a column (indicative of an equilibrium state where foam formation by bubbling compensates the foam collapse). The influence of the dilution with demineralized water was also taken into account. A foaming liquid constituted with Ecopol from Bio-ex diluted with 60% of water was eventually chosen for its ability to produce a wet foam dense and stable enough, as illustrated in Fig. 2, which shows the temporal evolution of foam density for several Ecopol dilutions. The rheological behavior of the chosen foaming liquid was fully characterized. In particular, its apparent viscosity was measured at 100 ± 30 mPa s.

In the scope of this work, a given aqueous foam can be characterized by considering its density, mean bubble diameter, and sound velocity. These parameters were controlled before each test. Density can be evaluated either by weighting a foam sample or by measuring the foam conductivity. Both methods were used. For the

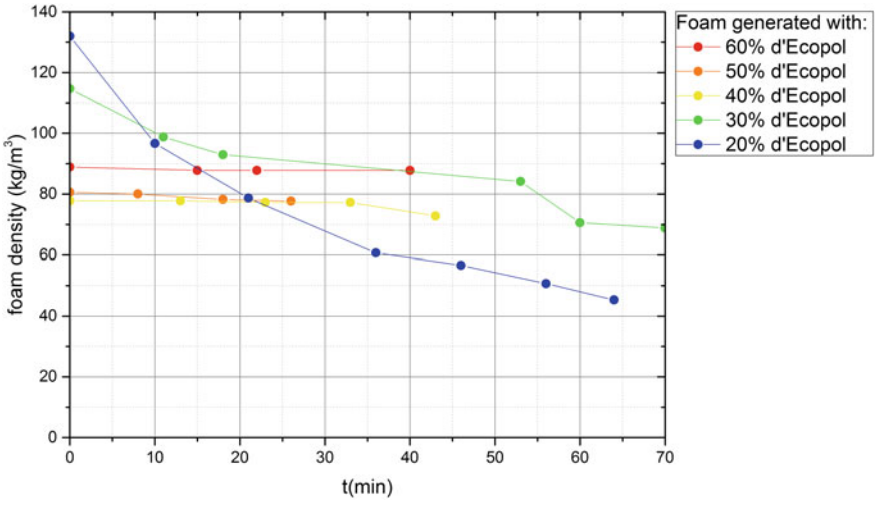

Fig. 2 Temporal evolution of the density of foams generated with different concentrations of foaming liquid

first one, 9.5 L foam samples were weighted with a Kern EMB balance, yielding a maximal incertitude of 20%. An empiric relation links the liquid fraction and the foam electrical resistance [25]. A setup constituted by a conductivity cell (two 8 cm^2 aluminum plates separated by a 4 cm gap) and a RLC Fluke PM6304 bridge (with 0.1% accuracy) was used to access the foam density. Foams are unstable. Three phenomena of foam aging are involved: drainage (under the gravity, the liquid in the foam flows along the skeleton composed by the gaseous bubbles), coarsening (the pressure in the small bubbles is higher than in their larger neighbors and they tend to empty the latter), and coalescence (the liquid film dividing two bubbles breaks). The foam stability can be measured by successive weightings of a drilled container that enables the drained liquid to be evacuated, or by conductimetry, which is more convenient. An average density can therefore be determined by conductimetry with this method and the designed cell.

Bubble diameters can be determined by taking a picture of a layer of bubbles dropped on a microscope slide. An example of such a picture is presented in Fig. 3. Pictures are then analyzed with the ImageJ image processing software which, assuming the bubbles are spherical (a sensible assumption for wet foams), yields the diameter distribution. The polydispersity coefficient p can then be calculated to evaluate the foam quality [25].

$$p = \frac{< R^3 >^{\frac{2}{3}}}{< R^2 >} - 1$$

with

R the bubble radius (m)
$< R >$ the average bubble radius of the foam sample (m)

Sound velocity in aqueous foams is a difficult topic, which is still debated. It is a common approach to evaluate it with the Wood model [26]. Recent works by Pierre et al. [27] highlighted the fact that the sound velocity in a foam varies widely as a function of several parameters, including the liquid fraction ϵ, the wave frequency, and the bubble mean diameter. Using the results provided in this paper, we could evaluate the sound velocity of the different foams used in our experiments. They vary between 25 m s^{-1} for the smallest bubbles (mean diameter 0.2 mm) and 275 m s^{-1} for

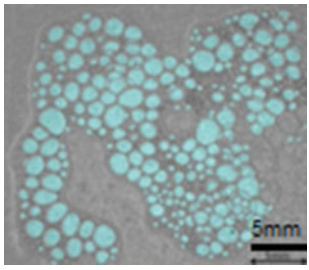

Fig. 3 Example of taken foam bubbles picture by camera and processed by ImageJ

Table 1 Main properties of the foams used in the blast and shock tube experiments

Device	Flow-focusing	Venturi
Uses	Shock tube tests	Pyrotechnic tests
Foaming liquid concentration	0 – 100%	6%
Foam density (kg.m^{-3})	40 – 60	15 – 50
Average bubble radius (mm)	0.2 – 1.4	0.2 – 0.4
Polydispersity coefficient	0.3	0.2

the largest ones (mean diameter 1.4 mm). The inverse of the pressure rising time in the shock wave was considered as the wave frequency.

Three systems were used to generate the foam according to the requirements specified in the beginning of this part. Large-scale experiments (blast experiments involving explosive charges, in the frame of the present study) require large volumes of foam. In this case, we resorted to a commercial system used by firemen and were able to obtain flow rates higher than 500 L/min. This system is based on the Venturi method and allows the generation of foams with a density between 15 and 50 kg m^{-3} while keeping a constant mean bubble radius of 0.3 mm. For small-scale experiments (shock tube tests), we designed two systems based on the classical flow-focusing method [5, 25], which consists in mixing air and foaming liquid through a Y connector. After this constriction, single bubbles are produced. To obtain large bubble foams, we resorted to a rake of Y connectors. To obtain smaller bubbles, a single generator was fitted with an array of 2 mm spheres positioned at the exit of the Y connector. With these systems, bubble diameter could be varied between 0.2 and 1.4 mm and density between 40 and 60 kg m^{-3}. The properties of the foams produced are summed up in Table 1, along with their respective average polydispersity coefficients, which are quite satisfying.

3 Spherical Shock–Foam Interaction

This part of our work studies the tridimensional propagation of the shock wave generated by a reference explosive charge in a wet foam volume with a density between 40 and 60 kg m^{-3}. Pressure gauges are placed in the foam at different distances from the charge. A stated previously, our aim is both to add to the existing experimental results and to establish a reference case for the study of the mitigation of the effects generated by the blast and fragments produced by an explosive device. Experiments were performed with C4 cylindrical charges placed at 10 cm from the ground in the center of a metallic enclosure shown in Fig. 4. The inner volume of the container is 6 m^3. C4 was chosen because it is easy to handle and to mold. Three pencil-type baseline 137A22 pressure gauges from PCB Piezoelectronics were located in the foam

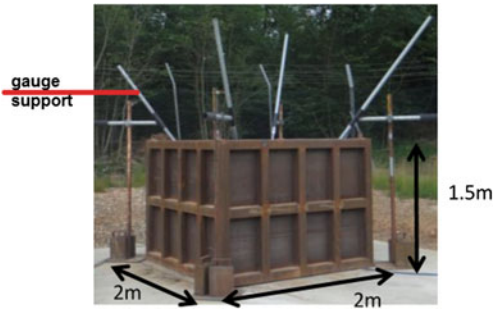

Fig. 4 Blast experimental setup

at respective distances of 0.8, 1.1, and 1.4 m of the center of the charge. Charges of 300 and 700 g were detonated to vary the blast overpressure.

Three tests were performed with a 300 g charge and without foam in order to assess the experimental reproducibility and to provide a reference case, since the partially confined configuration is not standard. The pressure profiles obtained from the three gauges are shown in Fig. 5, with each color corresponding to one test. The first part of the profiles is straightforward to analyze: a first peak corresponding to the

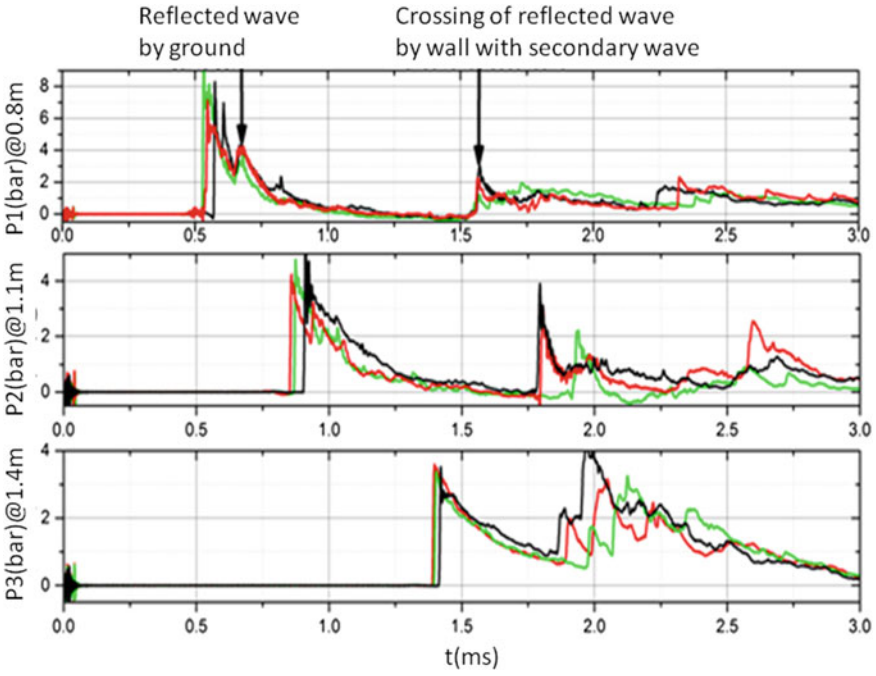

Fig. 5 Temporal evolution of the overpressure for gauges 0.8, 1.1, and 1.4 m from a bare 300 g C4 cylindrical charge for three different tests

incident blast wave is followed by a second one corresponding to the wave reflected on the walls of the confinement. The following parts of the signals are indicative of the multiple-wave reflections in the enclosure. The incident overpressure was compared with reference data from Kinney and Graham [28] and computational results (obtained with ANSYS Autodyn) with good agreement. As can be seen from these results, the reproducibility is satisfying, with variations in overpressures and times of arrival below 20%.

Given the scale of the setup and the generating device used, measuring the bubble size did not make sense. As stated in Table 1, the generating device was tested before the experimental campaign, showing that the average bubble size did not significantly vary and was about 0.3 mm. Therefore, only the average density was controlled before each shot. The overpressures measured with foam for both charges are shown in Fig. 6. Contrary to the case of the bare charge, no significant reflected wave can be seen on these signals, which highlights the damping capacity of the foam. Furthermore, the incident overpressure exhibits the usual double structure (cf. Fig. 1). Although the overpressures recorded for the 700 g C4 charge remains sharper for a longer time, both signal eventually take the bell profile associated with the main compression phase in the fragmented foam. The profiles were post-processed, in order to determine the time of arrival of the incident wave t_a, the duration $t_p - t_a$ and overpressure P_p of the precursor wave and the duration $t_c - t_p$ and overpressure P_c of the compression wave. Wave diagrams were plotted (not shown here, but t_a, t_p, t_c, P_p and P_c are indicated in Fig. 6). The evolution of the recorded overpressure P_c as a function of scaled distance Z was compared with the recently published experimental results of Del Prete et al. [5] and with the aforementioned empirical formulas by Hartman and Larsen [2, 29] (cf. Fig. 7). Overall, the maximal overpressure P_c is decreased by 90% for the shortest scale distances considered in this study, and up to

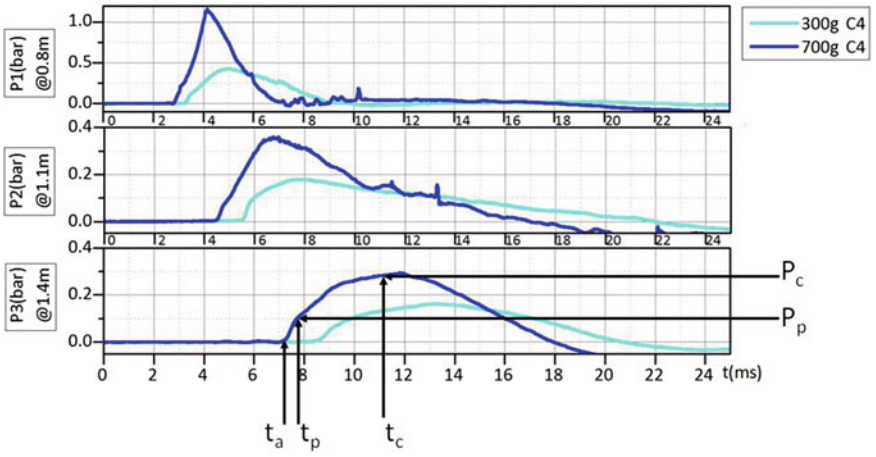

Fig. 6 Temporal evolution of the overpressure for gauges 0.8, 1.1, and 1.4 m from 300 and 700 g C4 cylindrical charges in aqueous foam

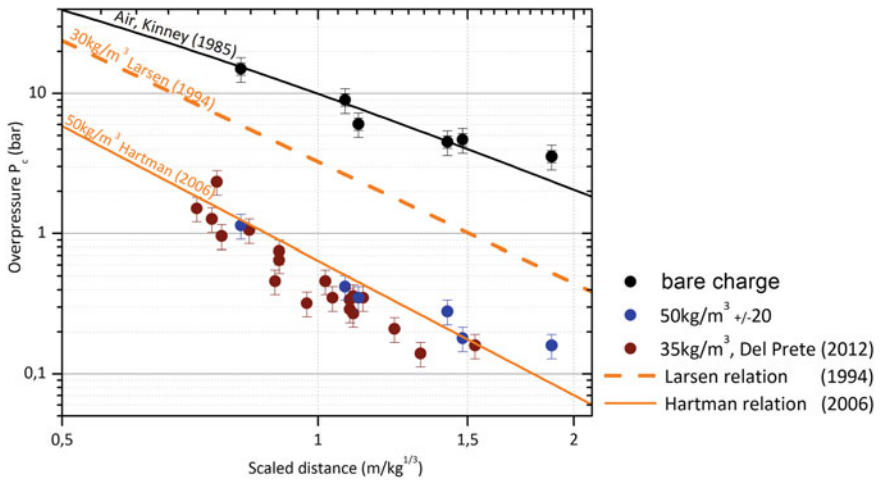

Fig. 7 Maximal overpressure P_c as a function of scaled distance for different aqueous foams and different charges

95% for the largest ones. Comparing our data with those of Del Prete et al. [5] does not permit to draw any conclusive result regarding the influence of the foam density on the blast mitigation. Besides, other factors (such as the mean bubble diameter) must also be taken into account.

Figure 8 shows the evolution of the precursor wave overpressure as a function of the scale distance. Here again, our results follow the same trend as those from

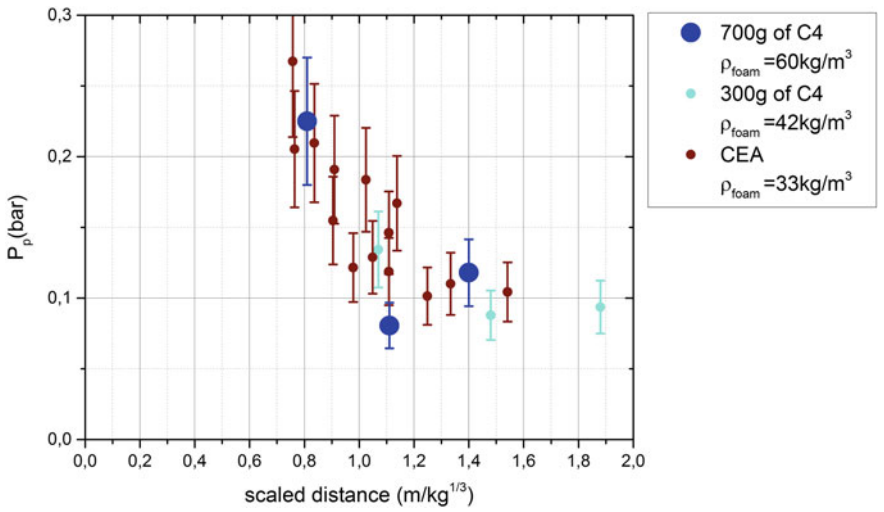

Fig. 8 Maximal overpressure of the precursor wave P_p generated by an explosive charge in a liquid foam as a function of the scaled distance Z for our experiments and those of the CEA [5]

Del Prete et al. [5]. The precursor overpressure varies between 0.1 and 0.3 bar. It decreases with the scale distance, which can be attributed both to the blast attenuation and to the spherical wave propagation. It is not possible to discriminate the influence of either effect. The precursor velocity was post-processed from the pressure signals, and satisfactorily compared with a simple empirical relation provided by Gelfand [6]. The fragmentation duration $t_p - t_a$ varies between 400 and 1400 µs. It is slightly larger than the duration observed by Del Prete, which seems coherent, since our foam has a larger density. This duration increases with distance, which could be explained by the diminution of the precursor overpressure with distance.

4 Planar Shock–Foam Interaction and Study of the Bubble Size Influence

For this part of our study, we used a shock tube with a length of 3.94 m and an inner square section of $80 \times 80\,\text{mm}^2$. The high-pressure section is 0.8 m long and separated from the low-pressure section by a Mylar diaphragm (100 to 225 µm thick). The tube was fitted with six PCB 113B21 piezoelectric pressure gauges as shown in Fig. 10. The end section was filled with about 3 L of foam, leaving two pressure gauges (P1 and P2) outside the foam. Two shock wave Mach numbers were studied: 1.4 and 1.6. Bubble size (depending on the foam generating system used, cf. Sect. 2) and foam density were systematically controlled before each shot. As in the previous case, reproducibility was thoroughly tested, both with and without foam. In the case of an incident shock Mach number of 1.6, the pressure profiles obtained with each gauge are shown for the small bubble foam (SB) and large bubble foam (LB) in Fig. 11. Two equivalent tests are considered for each configuration. It appears that reproducibility is very good in the initial stages of the phenomenon. Discrepancies then appear, which can easily be attributed to the differences in the foam density from one test to the other, and, in some extent, to some nonuniformity in the foam volume. This is particularly true for the large bubble foam, which is arduous to produce. Figure 11 highlights one shortcoming of our experiments. When comparing the profiles obtained for each foam, they seem to exhibit a different structure, with a peak beginning at t = 2 ms observed only with the large bubbles. This is classically observed in shock tube experiments, and is due to the shock wave R_m reflected at the extremity of the test section (see Fig. 9). This reflected shock wave is then attenuated by the rarefaction propagating from the driver section. In the case of the small bubbles, the velocity of the incident shock wave decreases more than with large bubbles. It takes therefore more time for the reflected wave to reach the pressure sensors, and the interaction with the rarefaction wave occurs almost simultaneously. Therefore, only the very beginning of the pressure rise caused by the reflected shock wave can be recorded. This implies that the phenomena occurring in each foam are not fundamentally different, contrary to what the pressure recordings would suggest.

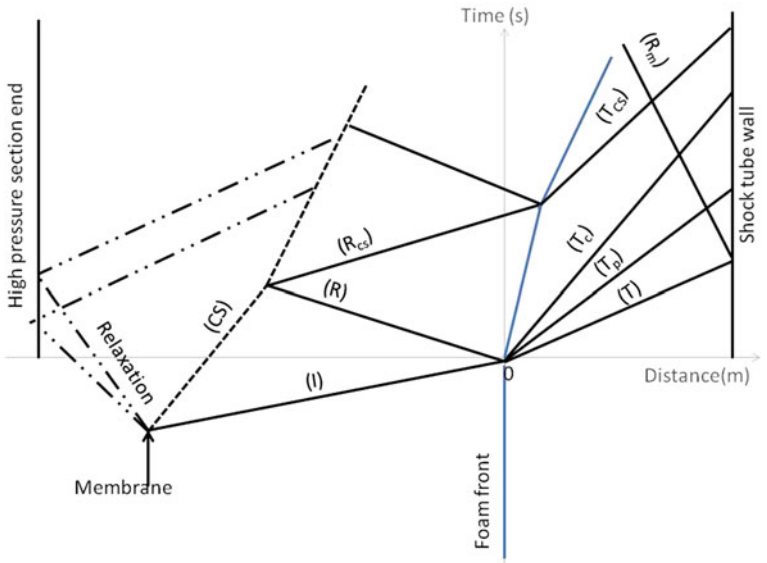

Fig. 9 Theoretical wave diagram for a shock tube partly filled with aqueous foam

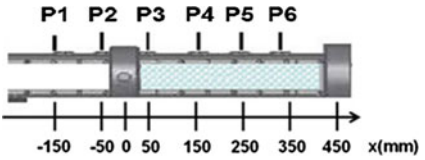

Fig. 10 Positions of the pressure gauges in the shock tube test section

Sensors P1 and P2, which are outside the foam, show similar signals and evidence P_r, the maximal reflected pressure at the air–foam interface (associated with wave R in Fig. 9). When the incident shock wave I meets the air–foam interface, a shock wave is reflected and propagates toward the driver section. This is due to the impedance mismatch at the interface. The sound velocity in the small bubbles is much lower than in the large bubbles (cf. Sect. 2). The acoustic impedances follow the same trend, which accounts for the difference in the transmitted overpressures. The overpressure of wave T transmitted in the foam is close to the one of the reflected shock wave. In the foam, the double structure of the wave front is again recorded for this experimental configuration.

The velocity of the transmitted shock wave V_{ta} was determined from the pressure profiles (Fig. 12), highlighting the fact that the wave is more decelerated in the small bubbles. This can intuitively be attributed to the fact that, in this case, the wave needs to cross more liquid films per unit volume, and is consistent with Britan's conclusions [8]. It can be seen that for small bubbles, the wave velocity seems to reach a constant value (around 100 m s^{-1}) independent of the Mach number of the incident wave. This velocity is also significantly different from the estimated sound

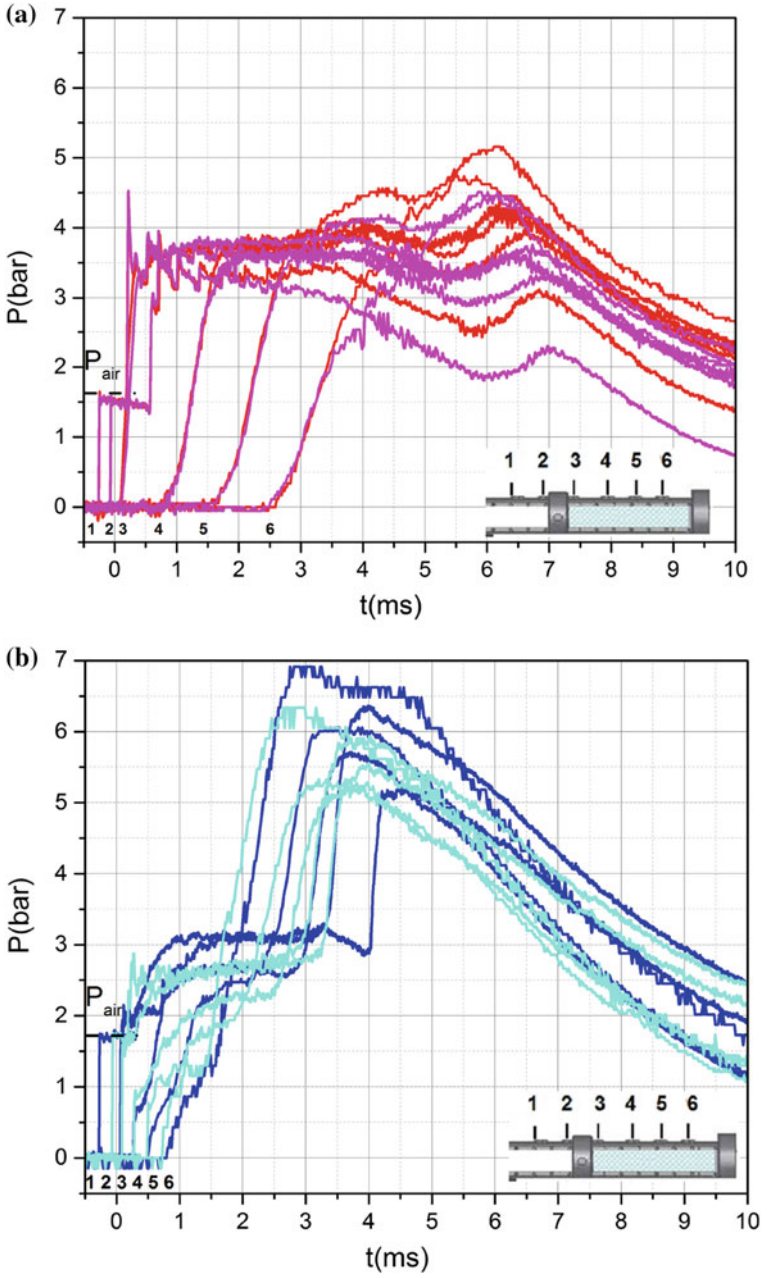

Fig. 11 Temporal evolution of the overpressure for the interaction between a M = 1.6 shock wave and an aqueous foam—**a** Small bubbles—**b** Large bubbles

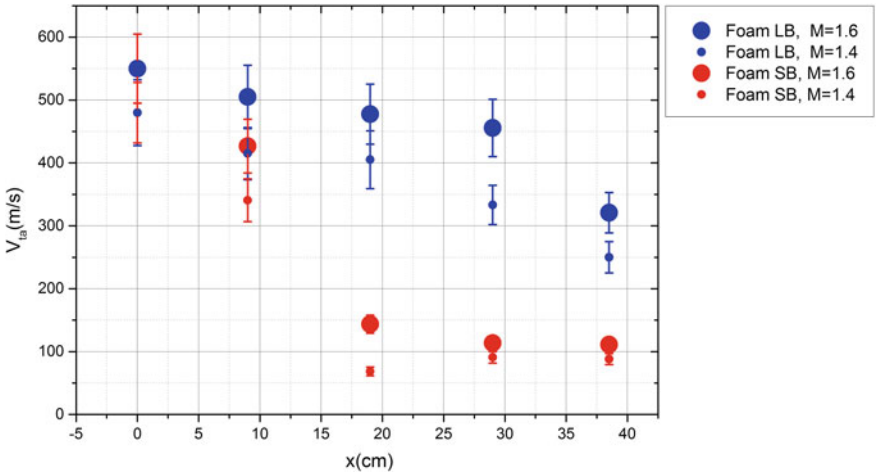

Fig. 12 Spatial evolution of the wave velocity in an aqueous foam as a function of wave Mach number and bubble size

velocity in the small bubble foam (25 m s^{-1}). It seems that the same behavior is not observed for large bubbles. It can also be noted that the concavities of both $V_{ta}(x)$ curves are not the same, although we so far have no explanation for this.

The evolution of the precursor in the large bubbles is also worth noticing. As shown in Fig. 13, it exhibits a large amplitude (initially larger than 1.5 bar, instead of the few kPa usually recorded), which is usually observed with dry foams. It is also

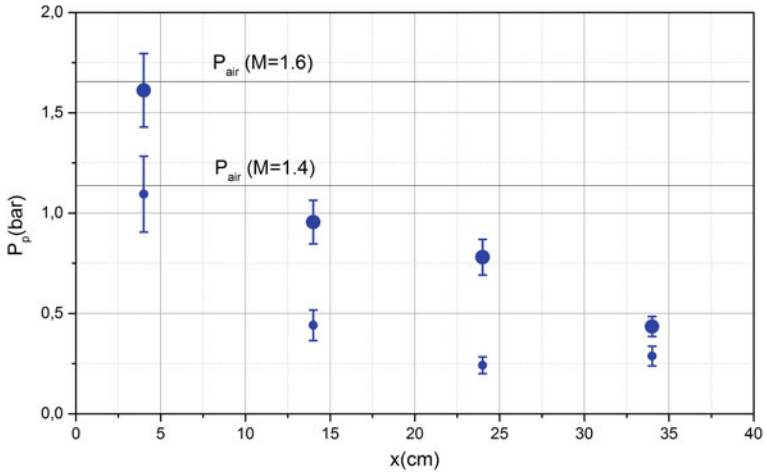

Fig. 13 Spatial evolution of the overpressure of the precursor wave as a function of Mach number for a large bubble foam

strongly attenuated as it propagates, which is not observed for more usual bubble radii (up to 0.5 mm). Further analysis of this peculiar behavior requires a local study of the wave front focused on the dynamic interaction of a shock wave and a series of aqueous films. To our knowledge, such a study is not available in the open literature.

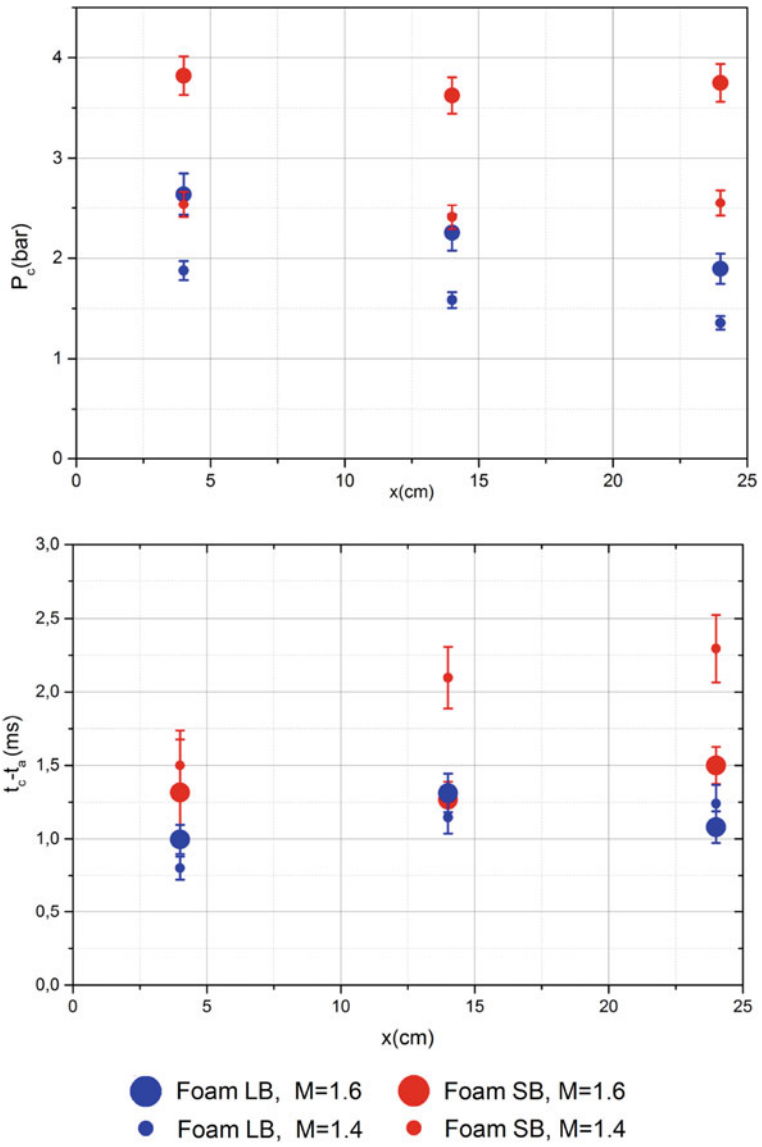

Fig. 14 Spatial evolution of the overpressure and duration of the compression wave as a function of Mach number and bubble size

The progressive rise from the precursor pressure P_p up to the equilibrium pressure P_c corresponds to a relaxation zone in which momentum and energy are transferred between the liquid and gas phases [8]. The evolution of the compression pressure P_c as a function of distance is plotted in Fig. 14 for the two Mach numbers and the two kinds of foam considered. For the small bubbles, this equilibrium pressure seems to tend toward the reflected pressure at the air–foam interface. Pressure P_c is lower in the large bubbles, and seems to keep decreasing as the wave propagates, showing that an equilibrium state has not been reached in this case. Pressure P_c seems to be less sensitive to Mach number in this case. Some differences can also be noticed as regards the duration of the compression phase. For the small bubbles, it keeps increasing and is very sensitive to the incident wave Mach number. This behavior is consistent with the previously published observations. On the contrary, in the case of the propagation in the large bubble foam, the overpressure duration reaches a limit value (around 1.25 ms) and seems almost insensitive to Mach number (over the considered range).

The pressure profiles recorded in both foams, along with the reference case in air, are plotted in Fig. 15 for M = 1.6. Owing to the impedance adaptation at the air–foam interface, an equilibrium overpressure higher than double the incident pressure is reached in the small bubble foam. This pressure is constant until the arrival of either of the waves reflected at the tube extremities. In this case, the mitigation can

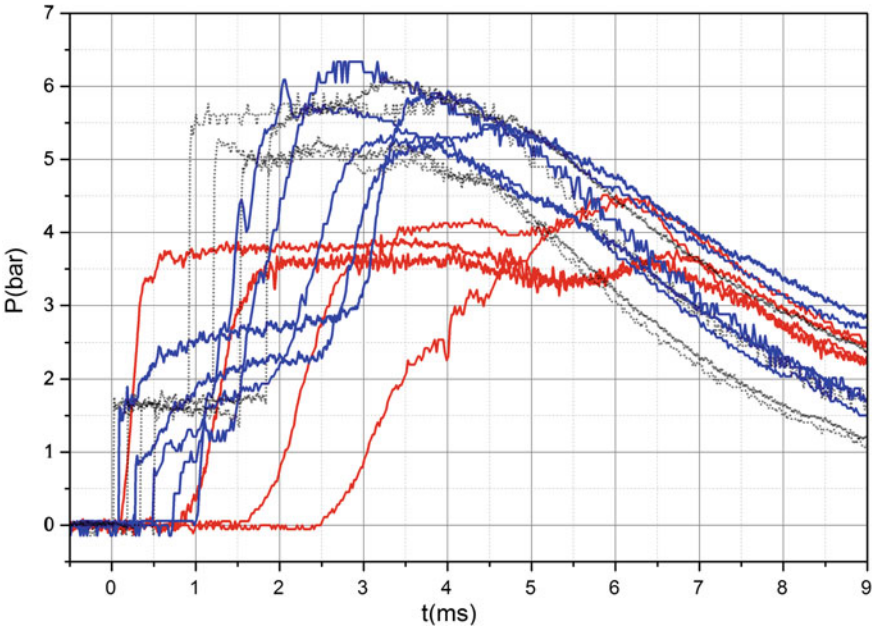

Fig. 15 Comparison of the overpressure profiles for a M = 1.6 shock wave in air (gray) and small bubble (red) and large bubble (blue) foams

be obtained because of the progressive attenuation of the pressure gradient as the wave travels in the foam. For the large bubbles, the overpressure increases by about 50% when the incident shock wave enters the foam. No precursor can initially be seen (i.e., the wave remains sharp). As the wave propagates in the foam, the double structure is recovered, with a precursor wave decreasing strongly. In this case, no equilibrium pressure can be reached. The wave also propagates much faster than in the small bubbles. Mitigation can nonetheless be obtained because the amplitude of the transmitted wave eventually decreases below the one of the incident wave and because the attenuation of the precursor generates a smoother wave front.

5 Conclusions

In this work, we have studied two reference configurations concerning the mitigation of shock waves by wet aqueous foams: spherical (blast wave) and planar (normal shock wave) propagation. Great care has been taken to accurately control the experimental conditions, in particular regarding the aqueous foam. A comparative study was conducted to select an appropriate foaming liquid and foam generation devices were designed in order to vary the mean bubble size. The foam properties (density and mean bubble diameter) were systematically measured before each test. In the case of blast wave attenuation, the results obtained are in good agreement with those already available in the literature. As regards the planar shock wave–foam interaction, two significantly different bubble sizes were considered (0.2 and 1.4 mm). It is to be noted that the 1.4 mm is a very unusual bubble diameter in the case of aqueous foams. The tested foams exhibited very different behaviors. For small bubbles, an equilibrium overpressure in the foam could always be reached, albeit at a noticeably larger value than the amplitude of the incident wave. The evolution of the wave in the large bubbles seems more complex. No equilibrium state seems to be reached, but the transmitted overpressure eventually decreases to a value close to the initial amplitude. As regards the evolution of the pressure gradient in the foam, it is strongly mitigated for small bubbles. Mitigation is longer to achieve for larger bubbles, and the wave initially remains very sharp. Although the wave propagates faster in the large bubble foam, it seems that, in the frame of this work's experimental conditions, it is at least as efficient to attenuate a planar shock wave. This macroscopic study raises quite a number of questions, which can only be answered by considering a more local experimental approach. The small-scale study of the interaction of a shock wave and a mock foam constituted by a series of interconnected aqueous films seems to be the logical continuation of this work.

References

1. Winfield, F.H., Hill, D.A.: Preliminary results on the physical properties of aqueous foams and their blast attenuating characteristics. Suffield Technical Notes, Defense Research Establishment, Suffield, Ralston, Alberta (1977)
2. Hartman, W., Boughton, B., Larsen, M.: Blast mitigation capabilities of aqueous foam, Technical report SAND2006-0533, Sandia National Laboratories (2006)
3. Domergue, L., Nicolas, R., Marle, J.-C., Mathey, L., Daloisio, M., Buche, L., Hubert, C.: Shock wave attenuation in aqueous foam. In: 3rd International Conference on Safety and Security Engineering, Inbook Series: WIT Transactions on the Built Environment,Safety and Security Engineering III, Rome, Italy, vol. 108, pp. 83–92 (2009)
4. McCallen, R.C. et al.: SERDP Munition Disposal source characterization pilot study, UCRL-CR-121838, Lawrence Livermore National Laboratory (1995)
5. Del Prete, E., Chinnayya, A., Domergue, L., Hadjadj, A., Haas, J.-F.: Blast wave mitigation by dry aqueous foams. Shock waves **23**(1), 39–53 (2012)
6. Gelfand, B.: Blast Effects Caused by Explosions (2004)
7. Raspet, R., Griffiths, S.K.: The reduction of blast noise with aqueous foam. J. Acoust. Soc. Am. **74**(6), 1757–1763 (1983)
8. Britan, A., et al.: Macromechanical modeling of blast-wave mitigation in foams. Part I: review of available experiments and models. Shock Waves **23**, 5–23 (2013)
9. Ball, G.J., East, R.A.: Shock and blast attenuation by aqueous foam barriers: influence of barrier geometry. Shock waves **9**(1), 37–47 (1999)
10. Borisov, A.A., Gelfand, G.E., Kudinov, V.M., Palamarchuk, B.I., Stepanov, V.V., Timofeev, E.I., Khomik, S.V.: Shock waves in water foams. Acta Astronautica **5**, 1027–1033 (1978)
11. Britan, B., Ben-Dor, G., Shapiro, H., Liverts, M., Shreiber, I.: Drainage effects on shock wave propagating through aqueous foams. Colloids Surf. Physicochem.Eng. Asp. **309**, 137–150 (2007)
12. Kudinov, V.M., Palamarchuk, B.I., Vakhnenko, V.A.: Attenuation of a strong shock wave in a two-phase medium. Sov. Phys. Dokl. **28**(10), 842–842 (1983)
13. Goldfarb, I.I., Shreiber, I.R., Vafina, F.I.: Heat transfer effect on sound propagation in foam. J. Acoust. Soc. Am. **92**, 2756 (1992)
14. Ranjan, D., Oakley, J., Bonnazza, R.: Shock-Bubble interactions. Ann. Rev. Fluid Mech. **43**, 117–140 (2010)
15. de Krasinski, J.S.: Some aspects of the fluid dynamics of liquid-air foams of high dryness fraction. Prog. Aerosp. Sci. **29**, 125–163 (1993)
16. Mallock, A.B.: The damping of sound by frothy liquids. Proc. Roy. Soc. Ser. A **84**, 391–395 (1910)
17. Surov, V.S.: Comparative analysis of two foam models. Combustion, Explosion and Shock Waves, vol. 31, n 31 (1995)
18. de Krasinski, J.S., Khosla, A.: Shock wave propagation and attenuation in foams. In: Fifth Australian Conference, University of Canterbury (1974)
19. Weaver, P.M., Pratt, N.H.: Experiment study of shock structure in aqueous foams and the unsteady shock emergence at a foam/air boundary. AIP Conf. Proc. **208**, 819 (1990)
20. Igra, O., Shreiber, I.: Formation of shock waves in gas-liquid foams. shock Waves **5**, 189–192 (1995)
21. Miura, H.: Weak Shock Waves in a liquid containing gas bubbles. J. Phys. Soc. Jpn. **32**(3) (1972)
22. Weaver, P.M., Pratt, N.H.: An experimental Investigation of the mechanisms of shock wave aqueous foam interactions. In: Proceedings of the International Symposium on Shock Tubes and Waves. VCH, Aachen, Germany (1988)
23. Zhdan, C.A.: Numerical modeling of the explosion of a high explosive charge (HE) in foam. Combust. Explos. Shock Waves **26**(2), 221–227 (1990)
24. Panczak, T.D., Krier, H.: Shock propagation and blast attenuation through aqueous foams. J. Hazard. Mat. **14**, 321–336 (1987)

25. Cantat, I., et al.: Les Mousses: Structure et Dynamique. Belin, Paris (2010)
26. Wood, A.B.: A Textbook of Sound. Bell, London (1944)
27. Pierre, J., Dollet, B., Leroy, V.: Resonant acoustic propagation and negative density in liquid foams. Phys. Rev. Lett. **112**, 148307 (2014)
28. Kinney, G.F., Graham, K.J.: Explosive Shocks in Air, 2nd edn. Springer, New York (1985)
29. Larsen, M.: Nest calculator, Technical report SAND94-2030, SANDIA National Laboratory (1994)